Journal of Photochemistry and Photobiology A: Chemistry 216 (2010) 250–255

Contents lists available at ScienceDirect

Journal of Photochemistry and Photobiology A: Chemistry

journal homepage: www.elsevier.com/locate/jphotochem

Photoreaction of ethanol on Au/TiO_2 anatase: Comparing the micro to nanoparticle size activities of the support for hydrogen production

M.A. Nadeem[a,b], M. Murdoch[a], G.I.N. Waterhouse[b], J.B. Metson[b], M.A. Keane[c], J. Llorca[d], H. Idriss[a,*]

[a] Department of Chemistry, University of Aberdeen, and School of Engineering, Robert Gordon University, Aberdeen, UK
[b] Department of Chemistry, University of Auckland, Auckland, New Zealand
[c] Department of Chemical Engineering, Heriot Watt University, Edinburgh, UK
[d] Institute of Energy Technologies, Technical University of Catalonia, Barcelona, Spain

ARTICLE INFO

Article history:
Available online 13 July 2010

Keywords:
TiO_2 anatase
Gold particle size
XPS Au4f
Ethanol IR
Ethanol TPD
Hydrogen production
Ethanol dehydrogenation
Ethanol dehydration
Photoreaction
Anatase nanoparticles
Anatase microparticles
Electron transfer

ABSTRACT

The work presents the dark and photocatalytic reactions of ethanol over Au particles deposited on TiO_2 anatase nano (≤10 nm) and micro (ca. 0.15 μm) particle catalysts. The Au particles are of uniform and similar dimension (mean particle size = ca. 5 and 7 nm on the micro- and nano-sized TiO_2, respectively). XPS Au4f indicated that in both cases Au particles are present in their metallic state with no evidence of charge transfer to (or from) the semiconductor. Under dark conditions, ethanol adsorption leads to stable ethoxide species (from *in situ* Infrared analysis) up to ca. 550 K at which point conversion to acetaldehyde by dehydrogenation and ethylene by dehydration occurs (from temperature programmed desorption (TPD) analysis). Liquid slurry photoreaction indicated the production of hydrogen with a rate ≈2 L/kg_{Catal} min on 2 wt.% Au/TiO_2 anatase nanoparticles under UV photo irradiation of comparable intensity to solar radiation. While the reaction rate per unit mass was lower on the micro-sized Au/TiO_2, it simply scaled up to an equivalent rate for the nano-sized Au/TiO_2 catalyst when normalised by unit area, indicating the absence of a particle size effect of the semiconductor on the electron transfer reaction within the range 10–150 nm).

1. Introduction

Many efforts are now devoted to finding processes for storing and/or converting solar energy. One mode of solar energy utilisation is the use of sunlight to generate energy carriers such as H_2 from renewable sources using semiconductor photocatalysts. Excitation of a semiconductor, such as TiO_2, with photons of appropriate energy produces an electron–hole (e^-–h^+) pair which may either recombine or react with appropriately adsorbed species. Photocatalysis with TiO_2 is a well-established field which exploits these phenomena, and which has been extensively reviewed [1]. Despite the appreciable number of published papers in this field [2], many crucial aspects of reaction mechanisms remain poorly understood. In the case of photocatalytic reaction over a semiconductor to generate hydrogen from a renewable source such as water or ethanol or a combination of both, the presence of a transition metal (TM) is required to facilitate e^- transfer from the conduction band to hydrogen ions to produce H_2.

The photoreactivity of TM-semiconductors materials, in general, depends on three key parameters: (i) the nature of the support; (ii) the nature and size of the TM; (iii) the surface structure of the support and its interface with TM. The polymorphic nature of a support such as TiO_2 has many effects, notably the variation in electron hole recombination rates as anatase is an indirect band gap while rutile is a direct band gap material. This affects the rate of electron–hole recombination making anatase (slow electron hole recombination rate) more active than the rutile polymorph [3–5]. The nature and size of the metal deposited also influences the electronic properties of the semiconductor. In the case of Au metal, a shift in the Fermi level closer to conduction band has been seen when decreasing the particle size from 8 to 3 nm [6]. The nature of the interaction of the metal with the support has been proposed to depend on the particle size of the support. This is, in part, because small support particles exhibit a higher percentage of surface defects that may interact further with the metal by charge transfer [7,8]. Moreover, charge transfer from the metal to the support increases with decreasing metal particle size as established in the case of Au on CeO_2 thin films [9].

Ethanol reaction over TiO_2 has been studied in some detail mainly with respect to photo-oxidation [10–13]. There has been sporadic work on hydrogen generation from ethanol over TM on TiO_2 [14–18]. TiO_2 exists in three forms: anatase, rutile and brookite. Most experimental work on polycrystalline photocatalytic materials uses TiO_2 Degussa P25 (80% A and 20% R) [19]. Some

* Corresponding author. Tel.: +44 1224 274503; fax: +44 1224 452921.
E-mail address: h.idriss@abdn.ac.uk (H. Idriss).

1010-6030/$ – see front matter © 2010 Elsevier B.V. All rights reserved.
doi:10.1016/j.jphotochem.2010.07.007

work was also conducted on pure A or R phases [20]. It has been reported that the photoreaction of organic compounds on metals impregnated on TiO_2 is sensitive to the metal loading [21–23] and some attempt has been made to correlate particle size with photoreaction efficiency [24]. However, work directed at the synthesis of TiO_2 nanoparticles [25,26] as novel photocatalytic materials has met with limited success. Both the particle size of the TM and the support may influence reaction rate, which can also be governed by the nature of the support (anatase versus rutile or a mixture of both) [27]. In this work, we have compared the photoreaction of ethanol to hydrogen on Au/anatase catalysts with similar Au particle size but with over one order magnitude difference in the particle size of the support. The work has involved IR and temperature programmed desorption (TPD) analysis for the dark reaction of ethanol in addition to photocatalysis for hydrogen production.

2. Materials and methods

Anatase nanoparticles were prepared by the sol-gel hydrolysis of Ti(IV) isopropoxide. Briefly, Ti(IV) isopropoxide (284.4 g) was dissolved in isopropanol (1 L) at 20 °C. Under vigorous stirring, milli Q water (1 L) was then added dropwise to the Ti(IV) isopropoxide solution resulting in the hydrolysis of the alkoxide and precipitation of hydrous titanium oxides. The final molar ratio of water: Ti(IV) isopropoxide in the reaction mixture was 55.5:1. The suspension was then left stirring for 24 h. The particles were subsequently collected by vacuum filtration, washed repeatedly with isopropanol, and then air dried for 2 days at 20 °C. Anatase nanoparticles were obtained by calcination of the dried powders at 400 °C for 2 h. The micron sized anatase powder used in this work was obtained from BDH chemicals.

Titania-supported gold nanoparticle catalysts were prepared by deposition-precipitation with urea (DPU). Under vigorous stirring, titania (2.5 g) was added to a 250 mL aqueous solution containing $HAuCl_4{\cdot}3H_2O$ (1.1 mM for Au loadings of 2 wt.%) and urea (0.42 M). The suspension of TiO_2 particles was then heated to 85 °C, and kept at this temperature under continuous stirring for 8 h. The Au(III) impregnated titanias were collected by vacuum filtration, washed repeatedly with milli Q water, dried for 2 days at 20 °C in a dessicator over silica gel, and then calcined at 300 °C for 1 h to thermally reduce surface Au(III) cations to Au metal.

XPS analyses were conducted on a Kratos Axis Ultra spectrometer using mono-chromatized Al Kα X-rays ($h\nu$ = 1486.6 eV) with the hemispherical electron energy analyzer operated in the hybrid lens mode. The take-off angle with respect to the specimen surface was 90°. The charge-compensating low-energy electron system was used to minimize specimen charging during X-ray irradiation. The binding energy scale was calibrated using adventitious hydrocarbon referencing (C1s = 284.7 eV). TEM data were collected at ANSTO (Sydney, Australia) using a JEOL 2010F TEM. Specimens for analysis were supported on carbon coated copper grids. XRD measurements were made using a Philips PW-1130 diffractometer, equipped with a Cu anode X-ray tube and curved graphite filter monochromator. Both catalysts were composed of pure anatase phase.

2.1. Catalytic method

The Au/TiO_2 catalyst (0.0065 g) was placed in a Pyrex tubular glass reactor (volume 98 mL) and heated to 400 °C with a H_2 flow rate of 5 mL min^{-1} for 15 h. The sample was cooled to room temperature under a H_2 flow that was switched to N_2 gas (O_2 free) for ca. 30 min. 15 mL of ethanol was injected via a septum into the glass reactor prior to UV irradiation. The catalyst and ethanol mixture were stirred continuously during the UV irradiation using a magnetic stirrer. The UV reactor consists of six 15 W black light UV tubes with a wavelength of 350 nm. The measured combined photon flux after a Pyrex glass of similar thickness to the reactor was found equal to 7 mW/cm^2 at a distance of 4 cm. Light from the sun has a flux of 100 mW/cm^2; therefore the photoreaction was conducted at flux that was roughly equivalent to solar radiation, assuming UV light represents ca. 5% of the total sun flux. Gas samples were taken every 20 min analysed using a TCD gas chromatograph (Shimadzu GC – 8A) equipped with a packed Porapak Q column for hydrogen, CO_2, methane, ethylene, acetaldehyde, methanol, water, ethanol and acetone. A second TCD gas chromatograph was used with He to monitor CO. Tests were conducted to establish linearity in terms of hydrogen production with increasing catalyst concentration to ensure that all photons were absorbed by the catalyst particles and that all particles had been illuminated. It was found that a catalyst concentration between 6 and 25 mg in the reactor exhibited a linear response.

2.2. Temperature programmed desorption (TPD)

TPD studies were performed using 50 mg of catalyst placed in a quartz U-shaped fixed bed reactor connected to a vacuum system. The vacuum system had a typical base pressure of 1×10^{-7} Torr maintained by a diffusion pump with a liquid N_2 trap. The whole system was connected to a Spectra Vision quadrupole mass spectrometer to monitor the masses of interest. The mass spectrometer had a mass range from 1 to 200 amu with a capability of monitoring 12 masses simultaneously when run in profile mode. Linear temperature ramping at 20 K min^{-1} was achieved by using an accurate temperature ramping unit which consisted of a Kaif digital temperature controller integrated with a glass lined furnace and a K type thermocouple. The thermocouple was inserted very close to the catalyst in order to accurately measure the catalyst temperature. Prior to TPD, the catalyst was H_2-reduced (1 atm) at 673 K for 4 h. Ethanol volumes ranged from 50 to 0.2 μL where the introduction of 2–5 μL was sufficient for surface saturation. The TPD presented in this work was conducted at saturation coverage. Ethanol was allowed to adsorb and equilibrate with the catalyst surface for 15 min. The reactor was pumped down (for 30 min) to remove any weakly held ethanol on the catalyst surface or reactor walls. The ethanol mass fragment m/z = 31 $(CH_2OH)^+$ was monitored until the measurement returned to baseline. Different mass fragments were recorded as function of temperature to monitor the desorption of products, i.e. ethanol (m/z = 31, 29, 45, 27), acetaldehyde (m/z = 29, 44, 15, 43), ethylene (m/z = 28, 27), methane (m/z = 16,15) water (m/z = 18,17), H_2 (m/z = 2), CO (m/z = 28, 16), CO_2 (m/z = 44). The desorbed products were determined by careful assignation of all mass fragment as a function of temperature, intensity and correlation with other mass fragment peaks. Any peak that could be assigned to a single product was first identified, recording the mass fragmentation pattern of the same pure product and subtracting the peaks from the TPD spectrum of the desorbed products. This approach is described in some detail elsewhere [28]. For quantitative analysis, peak area under was determined using the Trapezoidal method and the correction factor for the individual mass fragment peaks was calculated using the method described by Ko et al. [29]. Normalization of the individual mass fragments was achieved by multiplying the product desorption spectrum by the correction factor. Yield of each species as a fraction of the total desorbed component and % carbon selectivity as a fraction of total carbon desorbed were calculated as described elsewhere [30].

Infrared spectra were obtained using a Nicolet (Nexus) Fourier transform spectrometer. Infrared spectra of adsorbed species were obtained with a 256 scan data acquisition at a resolution of 4 cm^{-1}. Ethanol adsorption was performed in a stainless steel IR cell, equipped with removable CaF_2 windows (32 mm diameter, 4 mm thick) sealed with Viton O-rings. A type K thermocouple, welded

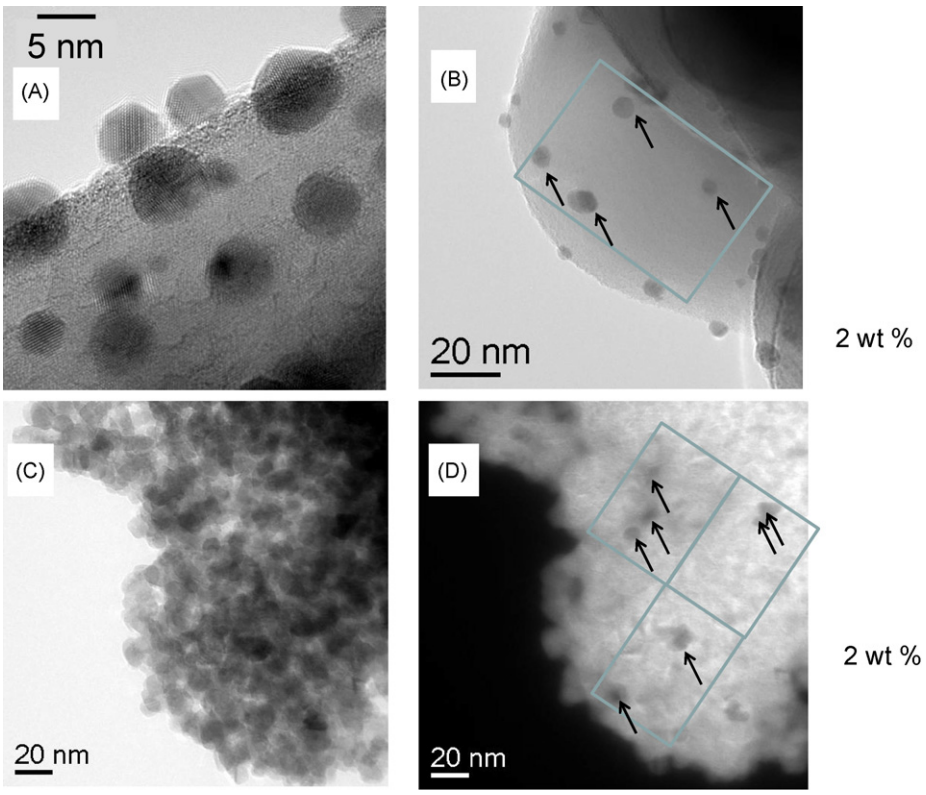

Fig. 1. TEM images of 2 wt.% Au/TiO_2 anatase microparticles (A and B) and of 2 wt.% Au/TiO_2 nanoparticles (C and D). Images A and B show two different areas of the microparticle catalyst at two different magnifications. Images C and D show the same area of nanoparticle catalyst conducted in bright and dark field modes to highlight the presence of Au particles (D). The arrows indicate unambiguous Au particles in images B and D. *Note*: the rectangles in images B and D are of the same size (45 nm × 65 nm).

into the centre of the cell in close proximity to the catalyst disc, was used to monitor the temperature. The catalyst samples were pressed into self-supporting discs (ca. 10 mm in diameter), and mounted into a gold-plated brass sample holder in the centre of the cell. The cell was then connected to a conventional vacuum line, and maintained at a base pressure (ca. 10^{-6} Torr) with a diffusion pump backed by a roughing pump. To obtain a clean surface the samples were annealed under 20 Torr of oxygen at 673 K followed by evacuation for 1 h. After cleaning the surface, the cell was allowed to cool to room temperature prior to the injection of ethanol via a septum connected to the IR cell which was separated using a valve after injection (varying amounts in 0.1 μL increments) and the cell was pumped down to at least 10^{-5} Torr to remove excess and loosely bound ethanol. The surface temperature was then raised in incremental steps to the final temperature, cooled to 300 K and the spectrum collected. The spectra presented in this work have been corrected by subtraction of the catalyst spectrum from that obtained post ethanol adsorption.

3. Results and discussion

3.1.1. Characterisation (TEM and XPS)

Fig. 1 presents representative TEM images of the two anatase supported Au catalysts. Both catalysts contain the same Au loading (2 wt.%) but the anatase support differs in that one is micro-sized and the other is at the nano-scale. The micro-sized anatase particles are ca. 0.15 μm in diameter while the nano-size particles are between 5 and 10 nm in diameter. These larger particles can be taken to represent bulk materials. The BET surface area is ca. an order of magnitude larger (105 m^2/g_{Catal}) for the nano-sized particles when compared with the micro-size particles (10 m^2/g_{Catal}); see Table 1 for more detail. Au particle sizes are however of comparable dimension for both catalysts, i.e. <7 nm. Fig. 2 presents XPS Au4f profiles for the two catalysts. In addition to the Au4f the Ti2p, O1s and C1s regions were scanned (not shown). Table 1 contains the ratios of Au to Ti for the two catalysts where it can be seen that the ratio is ca. three times lower for the nano-sized catalyst. This is due in part to the higher amount of TiO_2 analysed as the escape depth of the photoelectron is of the same order as the particle size in the nano-size particles while a large amount of Ti atoms are unseen in the micro-sized catalyst. A secondary factor is surface coverage of Au which is larger in the case of the micro-sized system.

3.1.2. Dark reactions: infra red and TPD studies

Ethanol adsorption has been studied by IR spectroscopy over TiO_2 and other oxides by many authors previously [31,32]. Here we focus on the modes of adsorbed species (recorded at 300 K) as a function of surface temperature under dark conditions using IR and TPD techniques. Fig. 3 presents IR spectra obtained after incremental exposures of the surface to increasing amounts of ethanol

Table 1
Surface and bulk properties of 2 wt.% Au/TiO_2 anatase nano and microparticles.

Catalyst	BET (m^2/g_{Catal})	XPS Au4f/Ti2p	Mean Au particle size (nm)	TiO_2 particle size (nm)
Au/TiO_2 (nano-)	105	0.016	ca. 7	ca. 10
Au/TiO_2 (micro-)	10	0.046	ca. 5	ca. 150

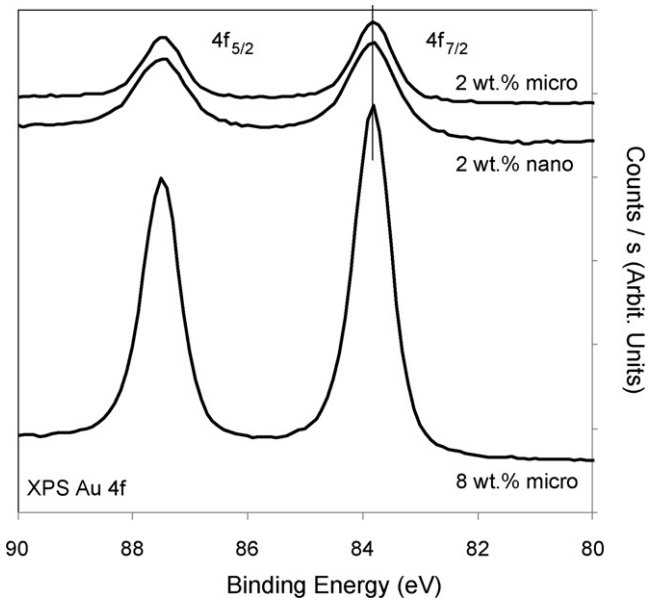

Fig. 2. XPS Au4f of 2 wt.% Au/TiO_2 anatase microparticles and 2 wt.% Au/TiO_2 anatase nanoparticles. The bottom spectrum is that of Au particles with large size (mean size >15 nm) as representative of bulk Au materials.

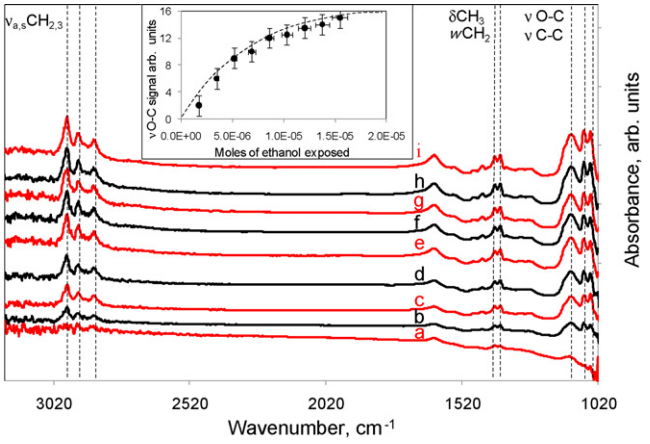

Fig. 3. FT-IR of ethanol irreversibly adsorbed on 2 wt.% Au/TiO_2 anatase nanoparticles at ca. 300 K with increasing exposures (a–i) to reach surface saturation; each increment corresponds to 0.1 μL injection of ethanol (1.7×10^{-6} mol).

at 300 K until saturation. Bands assigned to ν O–C and ν C–C of monodentate and bidentate ethoxide species are observed at 1150, 1110 and 1045 cm^{-1}, respectively. Table 2 presents the IR band assignment on 2 wt.% Au/TiO_2 anatase nanoparticles and compare them to those reported for pure TiO_2 anatase [31] and CeO_2 [32]. No noticeable difference is seen between the IR bands recorded in this work and those obtained for TiO_2 indicating that the presence of Au does not change the mode of adsorption of ethanol as

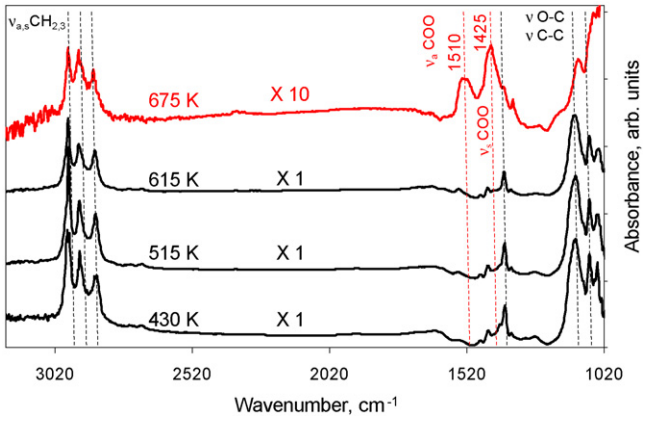

Fig. 4. Effect of temperature on the population of surface ethoxides and other minor reaction intermediates on 2 wt.% Au/TiO_2 anatase nanoparticles. The surface was first dosed with ethanol at 300 K, then heated to the indicated temperatures under dynamic vacuum for a few seconds and cooled to 300 K to collect the spectra.

seen by IR. The inset in Fig. 3 presents the peak height of the ν O–C mode of monodentate ethoxides with increasing exposure, until near saturation had been reached. Extrapolating the coverage at near saturation delivers a value of ca. 2×10^{-5} mol ethanol required for the 50 mg pellet of Au/TiO_2. From the BET surface area (see Table 1), we can estimate the total coverage of the surface to be ca. 0.2×10^{19} molecules per m^2. Because one m^2 contains about 0.5×10^{19} atoms of Ti, the ratio at this near saturation of ethanol to Ti is less than 1 and probably less than 0.5 (within experimental errors). Fig. 4 presents the effect of reaction temperature on ethoxide species. There is a steady but mild decrease of surface ethoxides up to 615 K, after which a sharp loss of surface ethoxide is seen. At 675 K, less than 10% of surface ethoxides is present, coinciding with the formation of surface carbonates. There were no other detectable stable intermediates. This indicates that reaction products observed during TPD (see below and Fig. 5) exhibit a weaker adsorption energy than ethanol and desorb upon formation. The reaction products were studied by temperature programmed desorption and are shown in Fig. 5. Ethanol TPD was performed on a H_2 reduced catalyst under continuous flow (1 atm) at 673 K. Fig. 5 represents the desorption profile of representative ion mass fragments of different products desorbed from the catalyst surface. The carbon yield and desorption temperatures of the main observed products are given in Table 3. The product profile is dominated by unreacted ethanol desorbing over a wide temperature range from 370 to 650 K with 60% of the total carbon yield. Ethanol desorption is due to recombination of ethoxides with hydrogen ions of the hydroxyls formed upon dissociative adsorption. It must be noted that IR analysis indicated that, below 675 K, the titania surface is mainly dominated by ethoxide species. Some of the hydroxyls formed upon ethanol dissociation to ethoxides are removed as water. Water desorption is also observed but because of inevitable background contribution, accurate quantitative values could not be determined. A marked desorption was observed over

Table 2
IR band assignments for ethanol adsorbed on Au/TiO_2 anatase nanoparticles with those reported in the literature for adsorption on TiO_2 anatase [31] and CeO_2 [34].

Modes	TiO_2 anatase [31] (cm^{-1})	Au/TiO_2 (this work) (cm^{-1})	Au/CeO_2 [34] (cm^{-1})
ν O–C/ν C–C	1150	1150 (shoulder)	1109
	1100	1120	1065
	1070	1070	1038
		1050	
δ CH_3	1360	1375	1362
ν_s CH_3	2875	2870	2875
ν_a CH_2	2930	2930	2933
ν_a CH_3	2975	2970	2971

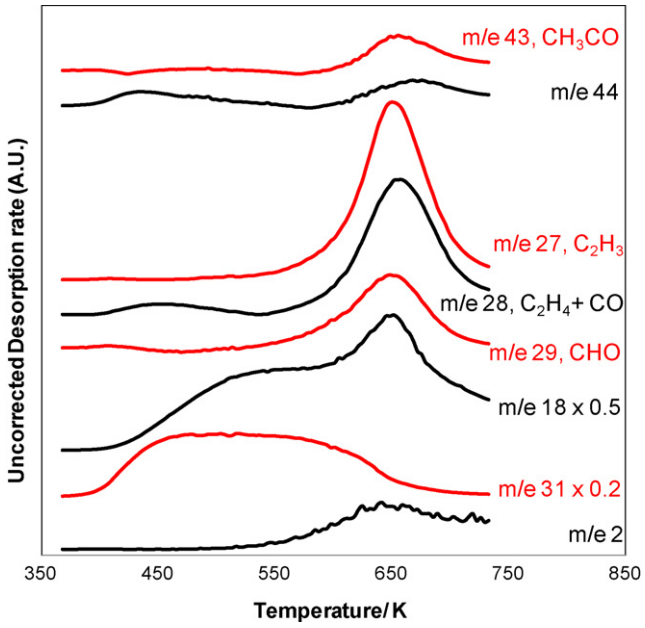

Fig. 5. Temperature programmed desorption after ethanol adsorption at saturation coverage at 300 K on 2 wt.% Au/TiO_2 anatase nanoparticles.

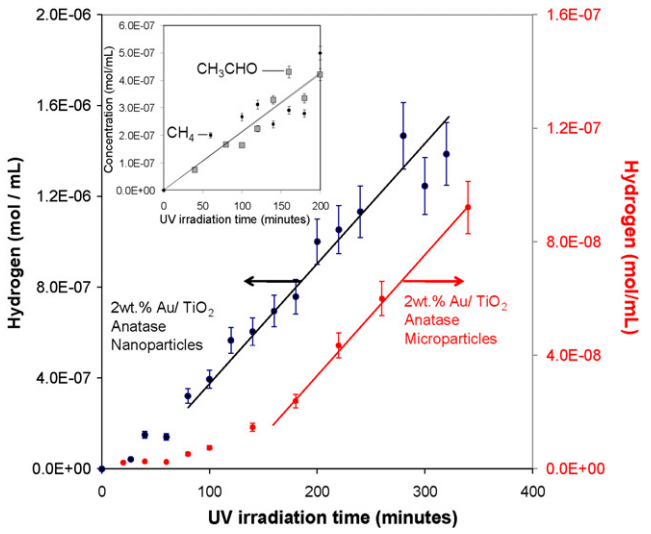

Fig. 6. Hydrogen formation as a function of time during the photocatalytic reaction of ethanol over 2 wt.% Au/TiO_2 anatase nanoparticles and 2 wt.% Au/TiO_2 anatase microparticles at 300 K. Catalyst concentration = 6.5 mg/100 mL.

the temperature range 650–670 K and this included ethylene, CO, CO_2, acetaldehyde and additional water. There was no or negligible desorption of methane as all *m*/*e* 15 and 16 were accounted for by acetaldehyde and CO_2 desorption, respectively. The ratio of the dehydrogenation to dehydration is ca. 2.

3.1.3. Photoreactions

Fig. 6 presents the reaction of ethanol to hydrogen as a function of UV irradiation time. The loading of both catalysts in the reactor was 6.5 mg/0.1 L, which ensured complete absorption of all photons by the catalyst as determined by the linear response of rate with loading (see Section 2). Three observations should be noted: (i) the induction period of the nano-sized particles is less that than corresponding to the micro-sized particles; (ii) the slopes of the lines once the induction period elapsed were roughly equivalent; (iii) the nano-sized catalyst shows a ca. one order of magnitude higher hydrogen production compared with the micro-sized system. When the data are normalised with respect to surface area both deliver a similar specific reaction rate. Normalisation to the Au/Ti ratio shows a deviation from that expressed per unit area for the reason invoked above; the escape depth covers Ti atoms in TiO_2 nanoparticles but not those in the microparticles. The mean particle size for Au deposited over TiO_2 nanoparticles is slightly larger (7 nm) for the f TiO_2 nanoparticles compared to the microparticles (5 nm). In both cases there are approximately 1.5×10^{16} particles per gram of catalyst (from the mass of Au, and the size of particles) yet as indicated in TEM the Au particles were well dispersed on the micro-sized TiO_2 support. These data indicate that reaction rate is insensitive to the particle size of the support, which in turn indicates that the reaction rate simply tracks the number of Au particles on the support.

Table 3
Product distribution and desorption temperatures associated with ethanol TPD from 2 wt.% Au/TiO_2 anatase nanoparticles.

Product	Peak temperature (K)	Carbon yield (%)
Acetaldehyde	650	5
Ethylene	650	10
Ethanol	375–725	75
Hydrogen	650	–
CO	650	<5
CO_2	650	<5
Water	440, 650	–

The other reaction products were monitored where the principal reaction is a dehydrogenation of ethanol to acetaldehyde:

$$CH_3CH_2OH \rightarrow CH_3CHO + H_2 \quad (1)$$

where some of the acetaldehyde is decomposed to CH_4 and CO; their concentration was monitored during the reaction. In the inset of Fig. 5 the change of the concentration of acetaldehyde and CH_4, in the case of Au/TiO_2 nanoparticle catalyst, as a function of time is given. One can estimate the initial product selectivity to avoid a significant contribution due to any unknown secondary reactions. For example, after 100 min of irradiation the product concentrations (in mol/mL) were as follows. H_2 (4×10^{-7}), CH_3CHO (1.5×10^{-7}), CH_4 (2.5×10^{-7}) and CO + CO_2 (5×10^{-7}). The build up of small amounts of CO_2 was always observed. It is possible that surface oxygen atoms participate in the reaction as indicated previously by other workers [22] although this was unlikely in our case as this would have resulted in catalyst deactivation. However, we have also detected (by TCD) trace amounts of water over time no matter how well the reactor was purged before the reaction. According to Eq. (1), one should expect an equimolar production of H_2 and CH_3CHO yet it appears that some of CH_3CHO is decomposed further to CH_4 and CO. In other words, the combined CH_3CHO and CH_4 (or CO) should be close to that of H_2. This is the case if the sum is done for CH_3CHO and CH_4 (4×10^{-7}) but deviates (probably above experimental error) if the sum is conducted for CH_3CHO and CO + trace CO_2 (6.5×10^{-7}).

Scheme 1 presents a plausible description of the photoreaction, where we focus on the first step of the reaction that involves ethanol to acetaldehyde and hydrogen. Upon UV excitation, electrons are transferred from the valance band to the conduction band. Most of these electrons–holes recombine. However, a fraction of the electrons at the conduction band are transferred to Au particles where H^+ ions may have migrated following the reaction of ethanol on the surface: ethanol to ethoxides (Eq. (1)) and ethoxides to α-hydroxyethyl radical (reaction (2a)) and acetaldehyde (reaction (2b)). During these two reactions an ethanol molecule has injected two electrons into the conduction band. The time lag between the two electrons injections from ethoxide to acetaldehyde is very fast in the case of TiO_2. If this time lag is slow the radical compound

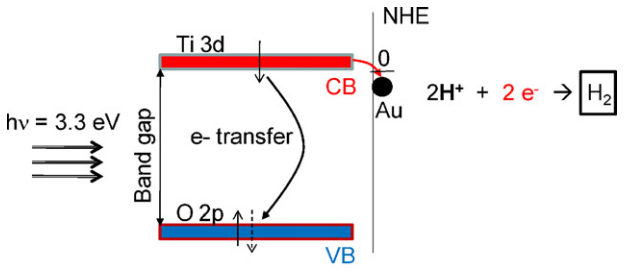

Scheme 1. A representation of the reactions involved in hydrogen production from ethanol over Au/TiO_2 under photo-excitation. The two hydrogen ions formed in reaction (1) and (2a) are reduced by two electrons upon their transfer from the conduction band to Au particles. Ethoxides inject two electrons into the valence band and acetaldehyde is consequently formed. The position of Au particles with respect to the conduction band is approximate as this varies with the particle size; see Ref. [6] for more detail.

made in reaction 2a may combine to give 2,3-butanediol as in the case of ZnS nanoparticles [33]. This compound was not detected in this study. Acetaldehyde once formed is removed since its adsorption energy is smaller than that of ethanol. While the adsorption energy of acetaldehyde compared to that of ethanol is not known for anatase surfaces, it has been shown that acetaldehyde desorbs from rutile at a lower temperature than ethanol, which is a strong indication of weaker adsorption energy. This may explain why we do not observe a significant conversion of acetaldehyde in our liquid slurry photoreactor. The normalisation of reaction rate by surface area may indicate that the electron transfer activity of anatase TiO_2 support is not influenced in moving from nano- to micro- (bulk) sized particles. One of the main properties that have been related to electron transfer within TiO_2 is the localisation versus delocalisation of the electronic wave function with the understanding that localisation decreases the e^-–h^+ recombination rate. Computation using hybrid Density Functional Theory (B3LYP), a method known to give acceptable band gap separation in TiO_2, of the electronic levels of the HOMO and LUMO of clusters of TiO_2 anatase ($Ti_{21}O_{70}H_{54}$) and rutile ($Ti_{23}O_{80}H_{68}$) has demonstrated [7] delocalisation unless electrons are injected into the clusters. Moreover, it was reported using a similar computational method that local defect states are only observed within the band gap for particles of 1 nm and less [8]. These two observations together with our experimental results indicate that nanoparticles of TiO_2 would need to be of 1 nm or less in order to effect any appreciable change in their electronic properties. In this case Au deposition would need to be of atomic size to ensure contact.

4. Conclusions

Ethanol is dissociatively adsorbed on Au/TiO_2 anatase to form ethoxides that are stable to relatively high temperatures under dark conditions. IR studies have indicated that these ethoxide species have the same ν-CO and ν-CC as those on TiO_2 alone. Above 600 K they react mainly to generate acetaldehyde and ethylene. Catalysts, composed of Au particles of about 5–7 nm size deposited on TiO_2 anatase, were found to be active for H_2 production from ethanol under photo-irradiation. This activity when scaled up corresponds to ca. 2 L H_2/kg_{Catal} min. With an increase in support particle size by over one order of magnitude (from $\leq$10 nm to ca. 150 nm), the activity per unit mass was lower but was equivalent for a normalisation based on surface area. This observation indicates that while nanoparticles of TiO_2 enhance the reaction, this effect is merely geometrical and does not result from any changes to intrinsic electronic properties.

References

[1] A. Fujishima, X. Zhang, D.A. Tryk, Surf. Sci. Rep. 63 (2008) 515.
[2] A. Kudo, Y. Miseki, Chem. Soc. Rev. 38 (2009) 253.
[3] R. Katoh, M. Mural, A. Furube, Chem. Phys. Lett. 461 (2008) 238.
[4] G. Rothenburger, J. Moser, M. Grätzel, N. Serpone, D.K. Sharma, J. Am. Chem. Soc. 107 (1985) 8054.
[5] D.P. Colombo, K.A. Russell, J. Saeh, D.E. Skinner, J.J. Cavaleri, R.M. Bowman, Chem. Phys. Lett. 232 (1995) 207.
[6] P.V. Kamat, J. Phys. Chem. C 112 (2008) 18737 (and references therein).
[7] V. Blagojevic, Y.-R. Chen, M. Steigerwald, L. Brus, R.A. Friesner, J. Phys. Chem. C 113 (2009) 19806.
[8] M.J. Lundkvist, M. Nilsing, P. Persson, S. Lunell, Int. J. Quant. Chem. 106 (2006) 3214.
[9] M. Baron, O. Bondarchuk, D. Stacchiola, S. Shaikhutdinov, H.-J. Freund, J. Phys. Chem. C 113 (2009) 6042.
[10] H. Idriss, E.G. Seebauer, Langmuir 14 (1998) 6146.
[11] T. Reztova, C.-H. Chang, J. Koresh, H. Idriss, J. Catal. 185 (1999) 223.
[12] P.M. Jayaweera, E.L. Quah, H. Idriss, J. Phys. Chem. C 111 (2007) 1764.
[13] Y. Mizukoshi, Y. Makise, T. Shuto, J. Hu, A. Tominga, S. Shironta, S. Tanabe, Ultrason. Sonochem. 14 (2007) 387.
[14] H.-L. Kuo, C.-H. Kuo, C.-H. Liu, J.-H. Chao, C.-H. Lin, Catal. Lett. 113 (2007) 7.
[15] Y. Wu, G. Lu, S. Li, J. Photochem. Photobiol. A: Chem. 181 (2006) 263.
[16] Y.Z. Yang, C.-H. Chang, H. Idriss, Appl. Catal. B: Environ. 67 (2006) 217.
[17] N. Strataki, N. Boukos, F. Paloukis, S.G. Neophytides, P. Lianos, Photochem. Photobiol. Sci. 8 (2009) 639.
[18] A.V. Korzhak, N.I. Ermokhina, A.L. Stroyuk, V.K. Bukhtiyarov, A.E. Raevskaya, V.I. Litvin, S.Y. Kuchmiy, V.G. Ilyin, P.A. Manorik, J. Photochem. Photobiol. A: Chem. 198 (2009) 126.
[19] G. Wu, T. Chen, X. Zong, H. Yan, G. Ma, X. Wang, Q. Xu, D. Wang, Z. Lei, C. Li, J. Catal. 253 (2008) 253.
[20] R. Abe, K. Sayama, K. Domen, H. Arakawa, Chem. Phys. Lett. 344 (2001) 344.
[21] M. Bowker, D. James, P. Stone, R. Bennett, N. Perkins, L. Millard, J. Greaves, A. Dickinson, J. Catal. 217 (2003) 427.
[22] L.S. Al-Mazroai, M. Bowker, P. Davies, A. Dickinson, J. Greaves, D. James, L. Millard, Catal. Today 122 (2007) 46.
[23] J. Greaves, L. Al-Mazroai, A. Nuhu, P. Davies, M. Bowker, Gold Bull. 39 (2006) 216.
[24] G.R. Bamwenda, S. Tsubota, T. Nakamura, M. Haruta, J. Photochem. Photobiol. A: Chem. 89 (1995) 117.
[25] R.R. Yeredl, H. Xu, Nanotechnology 19 (2008) 055706.
[26] E. Thimsen, N. Rastgar, P. Biswas, J. Phys. Chem. C 112 (2008) 4134.
[27] O. Carp, C.L. Huisman, A. Reller, Progr. Solid State Chem. 32 (2004) 33.
[28] A. Yee, S. Morrison, H. Idriss, J. Catal. 186 (1999) 279.
[29] E.I. Ko, J.B. Benziger, R.J. Madix, J. Catal. 62 (1980) 264.
[30] H. Idriss, K.S. Kim, M.A. Barteau, J. Catal. 139 (1993) 119.
[31] G.A.M. Hossein, N. Sheppard, M.I. Zaki, R.B. Fahim, J. Chem. Soc., Farad. Trans. 87 (1991) 2661.
[32] Z. Yu, S.S.C. Chuang, J. Catal. 246 (2007) 118.
[33] B.R. Miller, S. Majoni, R. Memming, D. Meissner, J. Phys. Chem. B 101 (1997) 2501.
[34] P.-Y. Sheng, G.A. Bowmaker, H. Idriss, Appl. Catal. A 261 (2004) 171.